kC cm^{-2} for single crystals[4] and our recent (unpublished) tests of 65 kC cm^{-2} on polycrystalline samples without decay. Extensive analysis of surface morphology and elemental distribution by SEM and WDS of the films could not identify the differences between films of different stability. At this stage we suspect the cause may be microscopic fissures, too small to identify by high-resolution scanning electron microscopy on the rough-appearing surfaces (Fig. 3).

The preparation of PEC cells is considerably less complex than PV cells, since the demanding step of evaporating a second semiconductor of controlled doping and good interface is replaced by the simple process of immersion in an electrolyte, later followed by an air anneal. The eventual maximum efficiency of this structure and its cost effectiveness have not yet been determined but the ability to create stable PEC cells based on thin films of $CuInSe_2$ is an important extension of the possibilities of exploiting the unique properties of the material.

The authors are grateful to Dr. R. Payling of B.H.P. Steel International Group, for assistance with scanning Auger measurements. This work was supported by The Australian Research Grants Scheme.

[1]R. A. Mickelsen and W. S. Chen, Appl. Phys. Lett. **36**, 5 (1980).
[2]L. L. Kazmerski, P. J. Ireland, O. Jamjoum, S. K. Deb, P. Sheldon, R. A. Mickelsen, W. Chen, and K. J. Bachmann, in *Proceedings of the 15th IEEE Photovoltaic Specialists Conference*, Denver, CO (IEEE, New York, 1981), p. 247; O. Jamjoum, L. L. Kazmerski, P. F. Russell, R. J. Matson, R. Ahrenkiel, P. J. Ireland, R. A. Mickelsen, W. S. Chen, and K. J. Bachmann, in *Proceedings of the 16th IEEE Photovoltaic Specialists Conference*, San Diego, CA (IEEE, New York, 1982).
[3]S. Menezes, Appl. Phys. Lett. **45**, 148 (1984); J. Electrochem. Soc. **131**, 2462 (1984).
[4]K. J. Bachmann, S Menezes, R. Kotz, M. Fearheily, and H. J. Lewerenz, Surf. Sci. **138**, 475 (1984).
[5]D. Haneman and J. Szot, Appl. Phys. Lett. **46**, 780 (1985).
[6]D. Cahen and Y. W. Chen, Appl. Phys. Lett. **45**, 746 (1984).
[7]Y. Mirovsky, R. Tenne, D. Cahen, G. Savatzky, and M. Polak, J. Electrochem. Soc. **132**, 1070 (1985).
[8]J. Szot and D. Haneman, Sol. Energy Mater. **11**, 289 (1984).
[9]T. P. Massopust, P. J. Ireland, L. L. Kazmerski, and K. J. Bachmann, J. Vac. Sci. Technol. A **2**, 1123 (1984).
[10]P. Corvini, A. Kahn, and S. Wagner, J. Appl. Phys. **57**, 2967 (1985); D. Cahen, P. J. Ireland, L. L. Kazmerski, and F. A. Thiel, J. Appl. Phys. **57**, 4761 (1985).

Spectroscopic measurements of He_2 in the afterglow of a dense Z-pinch plasma

J. E. Tucker, M. L. Brake, and R. M. Gilgenbach
Department of Nuclear Engineering, University of Michigan, Ann Arbor, Michigan 48109

(Received 30 September 1985; accepted for publication 4 December 1985)

Visible emission spectroscopy (330–650 nm) has been performed radially and axially on a Z-pinch plasma. During the peak compression, continuum and He II line emission (468.6 nm) predominated. We report the first observation of He_2 in the post-pinch phase of a dense helium Z-pinch discharge. Axial measurements of this afterglow plasma also revealed pronounced absorption bands which cannot be identified with He_2, He I, He II, or impurities.

Much of past work in Z-pinch plasma devices has been directed towards establishing hot, dense plasmas for the study of thermonuclear fusion.[1] More recently, the emphasis has been in producing reproducible x-ray sources[2] and overdense plasmas for laser interaction experiments.[3] Very little research has been reported in the cooling afterglow phase of the discharge which exists after the pinch disassembles. In this paper, we report the first observation of He_2 in the post-pinch phase of a dense helium Z-pinch plasma evolution.

The Z-pinch device used in this experiment has been reported elsewhere,[3] and is briefly reviewed here. The quartz discharge chamber had an inner diameter of 3.1 cm with elkonite electrodes located 15 cm apart. A copper coaxial current return path surrounded the quartz tube to minimize circuit inductance. The pinch was generated by discharging a 14-μF capacitor charged to 14 kV into the fill gas, which was 2.6 Torr of helium.

The maximum plasma compression (pinch time) was attained approximately 800 ns after the current initiation. A *p-i-n* diode monitored the frequency-integrated visible light emitted from the plasma, and had a maximum signal at pinch time. Double exposure, frequency doubled, ruby-laser holographic interferometry also established that the maximum electron density ($> 10^{19}$ cm^{-3}) occurred at this pinch time.[4] The pinch plasma lasted for approximately 200 ns, and often was seen to form a second pinch, 400 ns after the first pinch. The total duration of the current flow was about 20 μs. Soft x-ray emission measurements also have established that the pinch plasma reached a maximum temperature of 30 eV.[4] The duration of the soft x-ray emission from the discharge was over 1 μs.

Time-resolved visible spectroscopy measurements were performed with a 0.275-m, $f/4$ spectrometer using a 1200-g/mm grating, blazed at 400 nm. The spectrometer was coupled to a 1024 channel, gated, optical multichannel analyzer (OMA). The OMA and spectrometer were located inside a screened room to shield the OMA from electromagnetic interference.

Light emissions over the range of 330–650 nm were scanned as a function of time, however most of the investigation concentrated on the range of 380–480 nm. Radial emission measurements were performed at the chamber midplane through 0.9-cm access holes. The results of the radial measurements are shown in Fig. 1. In the figure, the positive

0021-8979/86/062251-03$02.40
© 1986 American Institute of Physics

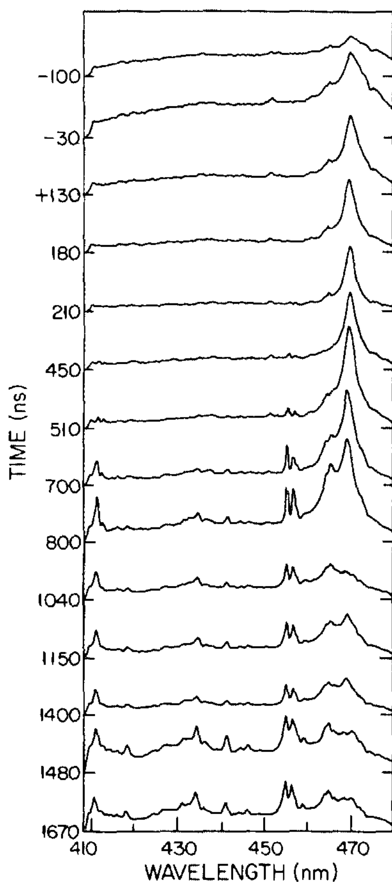

FIG. 1. Time-resolved spectra obtained radially with respect to the Z-pinch axis. Numbers on the ordinate refer to the time difference between the center of the OMA 170-ns gate width and the maximum pinch compression.

ordinate numbers indicate that the center of the OMA gate occurred after pinch time. The axial measurements are shown in Fig. 2, and were performed through holes located in the upper (ground) electrode. These holes also acted as the gas inlet to the chamber.

The results of the radial measurements showed a large emission peak at about 469 nm, which corresponded to the He II (3^2D-4^2F) transition. Stark broadening was the primary mechanism for the large width of the He II line. This width can be used to estimate the electron density in the discharge.[5] At pinch time, the Stark broadened width was over 15 nm, and corresponded to an electron density of more than 10^{19} cm^{-3}. This number agreed with the results of interferometry, which also gave spatially resolved electron density profiles. Between 500 and 800 ns after pinch time, the Stark-broadened He II linewidth corresponded to a constant electron density of about 10^{18} cm^{-3}. Holographic interferometry at these times showed a uniform electron density, but the magnitude of the density could not be established. After 800 ns, the intensity of the emission peaks due to He_2 ($2p\pi$-$4d\pi$ at 464 nm and $2p\pi$-$4d\sigma$ at 467 nm) became comparable to the He II line, making evaluation of the peak width due to the He II line impossible.

The background continuum peaked at pinch time, and was a result of bremsstrahlung and recombination radiation, both of which are strongly temperature and density dependent. An important observation at pinch time was that no other atomic emission lines, other than the He II 486.8-nm line, were detected in the spectrum. This indicated that the plasma was fully ionized, and that impurities were not present.

After pinch time, the background continuum level dropped off as the electron density decreased. Several emission peaks arose, particularly starting about 400 ns after pinch time. All of these peaks, other than the line mentioned above, were from He_2, and the main transitions are identified in Table I.[6] Neither He I nor contaminent spectra were seen, even for observation times greater than 4 μs after the pinch time.

The axial emission spectra were significantly different than the radial spectra. Most notably, the axial spectra were dominated by a bright continuum and several absorption bands. The principal emission peak in the axial spectra was the He II 469-nm peak. More He_2 band lines were present than in the radial spectra, although they were less prominent. The detected He_2 bands are presented in Table I.

The presence of absorption bands was a significant mea-

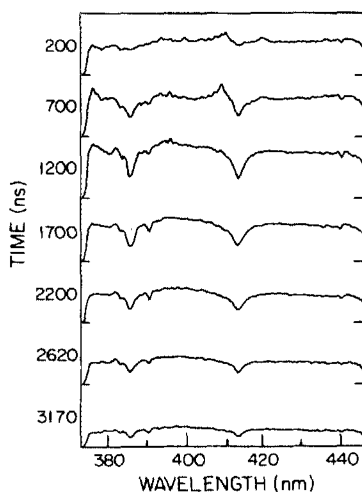

FIG. 2. Time-resolved spectra obtained parallel to the Z-pinch axis. Numbers on the ordinate refer to the time difference between the center of the OMA 600-ns gate and the maximum pinch compression.

TABLE I. Molecular helium emission bands and unpublished absorption bands measured in radial and axial spectroscopy.

Radial spectra		Axial spectra	
Line (nm)	Transition	Line (nm)	Transition
		377.7	Absorption peak
		382.6	Absorption peak
		384.8	Absorption peak
		387.4	Absorption peak
		389.7	Absorption peak
		392.7	$2s\sigma$-$4p\pi$
		398.5	$2p\pi$-$5d\pi$
		408.5	$2p\pi$-$5s\sigma$
410.7	$2s\sigma$-$4p\pi$	411.7	Absorption peak
		416.5	$2p\pi$-$5d\pi$
418.2	$2p\pi$-$4d\pi$	417.2	$2p\pi$-$4d\pi$
		417.7	Absorption peak
434.3	$2s\sigma$-$4p\pi$	434.5	$2s\sigma$-$4p\pi$
		437.1	$2p\pi$-$4d\delta$
		438	Absorption peak
441	$2p\pi$-$4d\delta$	441.2	$2p\pi$-$4d\pi$
444.4	$2p\pi$-$4d\pi$	443.6	Absorption peak
454.6	$2p\pi$-$4s\sigma$	451.1	$2p\pi$-$4s\sigma$
456.2	$2p\pi$-$4s\sigma$		
464.4	$2p\pi$-$4d\pi$	464	$2p\pi$-$4d\pi$
467.2	$2p\pi$-$4d\sigma$		
468.6	He II	468.6	He II
		472.9	Absorption peak

surement in the axial spectra. These bands did not correspond to any of the He_2 bands, nor did they correspond to any atomic transition of the materials present in the discharge chamber. Takao *et al.*[7] have seen absorption bands in a helium discharge when backlit by a xenon light source, however, these bands corresponded to He_2 transitions. In our experiment, the observed absorption bands may be due to He_2^+ transitions, however no emission or absorption spectra have ever been published for this molecule.

He_2^+ results from reactions involving He_2, which was present in the post-pinch discharge, as observed in emission spectroscopy above. He_2^+ will be created as a result of either inelastic impact ionization[8]

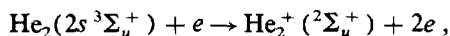

$$He_2(2s\,^3\Sigma_u^+) + e \rightarrow He_2^+(^2\Sigma_u^+) + 2e\,,$$

or by photoionization,[8]

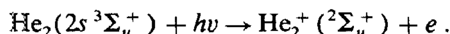

$$He_2(2s\,^3\Sigma_u^+) + h\nu \rightarrow He_2^+(^2\Sigma_u^+) + e\,.$$

Previously, the discharges in which He_2 has been observed, were much colder and less dense than our experiment, and these processes were ignored. The ionization energy of He_2 is approximately 23 eV, which is lower than the mean electron energy during the pinch. The electron temperature remained above 20 eV for more than 500 ns after the pinch time. A detailed kinetics code including currently unknown cross sections would be required to model the time behavior of the molecules, He_2 and He_2^+.

This project was funded by the National Science Foundation Grant Nos. ECS-8309682 and ECS-8504483, and the Presidental Young Investigator Award No. ECS-8351837.

[1]A. S. Bishop, *Project Sherwood—The U. S. Program in Controlled Fusion* (Addison-Wesley, Reading, MA, 1958).
[2]R. B. Spielman, D. L. Hanson, M. A. Palmer, M. K. Matzen, T. W. Hussey, and J. M. Peek, J. Appl. Phys. **57**, 830 (1985).
[3]D. G. Steele, P. D. Rockett, D. R. Bach, and P. L. Colestock, Rev. Sci. Instrum. **49**, 456 (1978).
[4]J. E. Tucker, Doctoral thesis (University of Michigan, Ann Arbor, Michigan, 1986) (unpublished).
[5]H. R. Griem, *Plasma Spectroscopy* (McGraw-Hill, New York, 1964).
[6]F. B. Orth and M. L. Ginter, J. Mol. Spectrosc. **64**, 223 (1977); F. B. Orth, C. M. Brown, and M. L. Ginter, J. Mol. Spectrosc. **69**, 53 (1978); D. S. Ginter and M. L. Ginter, J. Mol. Spectrosc. **101**, 139 (1983).
[7]S. Takao, M. Kogoma, T. Oka, M. Imamura, and S. Arai, J. Chem. Phys. **73**, 149 (1980).
[8]H. F. Wellenstein and W. W. Robertson, J. Chem. Phys. **56**, 1077 (1972).

Growth and properties of $Hg_{1-x}Cd_xTe$ on GaAs substrates by organometallic vapor-phase epitaxy

S. K. Ghandhi, I. B. Bhat, and N. R. Taskar
Electrical, Computer, and Systems Engineering Department, Rensselaer Polytechnic Institute, Troy, New York 12180-3590

(Received 25 September 1985; accepted for publication 16 December 1985)

Growth of epitaxial mercury cadmium telluride ($Hg_{1-x}Cd_xTe$) on (100) GaAs substrates by organometallic vapor-phase epitaxy is described. Transport measurements made on these layers at 80 K indicate an electron mobility greater than 2×10^5 cm^2/V s for layers of composition $x\cong0.2$. An intervening CdTe buffer layer was used to accommodate the large (14%) lattice mismatch between these systems, and HgCdTe layers have been grown with CdTe buffer layer thicknesses from 1000 Å to 3 μm. It is shown that a CdTe buffer layer of 2–3 μm is necessary to accommodate the misfit dislocations at the CdTe-GaAs interface.

$Hg_{1-x}Cd_xTe$ (MCT) is an important intrinsic semiconductor material for infrared detector applications, especially in the 8–16 μm range. Epitaxial growth of this material on a suitable substrate has received considerable attention in the past few years. CdTe is a natural choice as a substrate material because of its excellent lattice match and chemical compatibility with MCT systems. However, the lack of availability of high-quality, large-area CdTe substrates prompted many workers to consider alternate substrates such as GaAs, InSb, and sapphire. Of these, GaAs is especially important because it can serve as a window for backside illuminated devices. Moreover, its use opens up the possibility of integrating GaAs circuits with sensor devices of HgCdTe in a monolithic structure.

The growth of CdTe and MCT on GaAs substrates by molecular-beam epitaxy[1,2] (MBE) and organometallic vapor-phase epitaxy[3,4] (OMVPE) has been the subject of study in recent papers. In addition, we have reported on the electron channeling patterns and photoluminescence properties of CdTe grown on GaAs[5] by OMVPE. Our work has shown that, although the lattice mismatch between CdTe and GaAs is about 14%, high-quality single-crystal layers with featureless morphology could be obtained over the 350–420 °C range of growth temperatures. As an extension of this work, we report for the first time on the electrical characterization of MCT layers grown on GaAs substrates by OMVPE. These are grown with an intermediate buffer layer of CdTe in a continuous process. The effect of CdTe buffer layer thickness on the electrical properties of the MCT layer will also be discussed.

The epitaxial growth of CdTe and MCT was carried out in a system described previously.[6] Dimethylcadmium

 © 1986 American Institute of Physics